

Electromagnetic Shielding Triboelectric Yarns for Human–Machine Interacting

Shen Shen, Jia Yi, Renwei Cheng, Liyun Ma, Feifan Sheng, Huimin Li, Yihan Zhang, Chuang Ning, Hongbo Wang,* Kai Dong,* and Zhong Lin Wang*

Electromagnetic radiation, as one of the public hazards that injures human health and information safety, shall be shielded from the ambient environment. Here, by the virtue of polypyrrole polymerized polyamide yarns and silicone rubber, a yarn-based electromagnetic shielding-triboelectric nanogenerator (EMS-TENG) equipped with sensing ability is presented, which not only generates electricity from harvesting body motion energy but also serves as EMS to prevent electromagnetic interference. With the aid of knitting method, the developed EMS-TENG fabric exhibits the EMS effectiveness of 32.49 dB in 8.2–12.5 GHz and achieves a maximum instantaneous peak power density of $142.27 \mu\text{W m}^{-1}$. Furthermore, a real-time human-interactive system is developed by adopting the Internet of Things technology and EMS-TENG sensor. Based on the above, a simulated intelligent calculator with multiplication and division function is proposed, which can successfully translate electronic signals to digital numbers. With energy harvesting and self-powered sensing abilities, the EMS-TENG can convert mechanical energy into electrical signals from human movements. Looking forward, the EMS-TENG spurs an innovative technique toward a self-powered human-interactive sensing and functional protective textile for next-generation intelligent wearable applications.

the development is massive requirements in electronic devices/systems, in a total of billions to trillions, each of which needs electronic products.^[5–10] Inevitably, portable electrical components and complex circuits controlled by wireless network generate undesirable electromagnetic (EM) radiation.^[11–15] Thus, electromagnetic interference (EMI) is one of the most inevitable byproducts of modern electronics that severely threatens living environment and human health. Generally, fabrics, as the second skin for human beings, are regarded as the indispensable necessities for effectively protecting human from electromagnetic wave harm.^[16–18] However, benefiting from the fast development of technology as well as aiming to catering to the advancement of society, fabrics are gradually evolving towards intelligence instead of single performance. For that, the invention of variety smart sensors based on wearable fabric provides opportunities in both monitor service and identification by tracking of physiological signals. Thus,

taking impairment of human health into consideration, the demands for flexible, versatile, and wearable fabric with good EMI shielding and real-time sensing are highly desirable.^[19–22]

Sparked by the 5G technology, wearable products with flexibility and electronic functionality have underwent flourishing advancement in recent years.^[23,24] Smart fabrics, belonging to

1. Introduction

The fast development of electronic information and telecommunications with highly integrated circuits has caused severe electromagnetic radiation pollution, which endangers the daily life of human being and civil defense.^[1–4] A favorable merit of

S. Shen, H. Li, H. Wang
Jiangsu Engineering Technology Research Centre for Functional Textiles
Jiangnan University
No. 1800 Lihu Avenue, Wuxi 214122, P. R. China
E-mail: wxwanghb@163.com

S. Shen, J. Yi, R. Cheng, L. Ma, F. Sheng, Y. Zhang, C. Ning,
K. Dong, Z. L. Wang
CAS Center for Excellence in Nanoscience
Beijing Key Laboratory of Micro-Nano Energy and Sensor
Beijing Institute of Nanoenergy and Nanosystems, Chinese Academy of
Sciences
Beijing 100083, P. R. China
E-mail: dongkai@binn.cas.cn; zlwang@gatech.edu

R. Cheng, Y. Zhang, C. Ning, K. Dong, Z. L. Wang
School of Nanoscience and Technology
University of Chinese Academy of Sciences
Beijing 100049, P. R. China

Z. L. Wang
CUSTech Institute of Technology
Wenzhou, Zhejiang 325024, China
Z. L. Wang
School of Material Science and Engineering
Georgia Institute of Technology
Atlanta, GA 30332-0245, USA

 The ORCID identification number(s) for the author(s) of this article can be found under <https://doi.org/10.1002/aelm.202101130>.

DOI: 10.1002/aelm.202101130

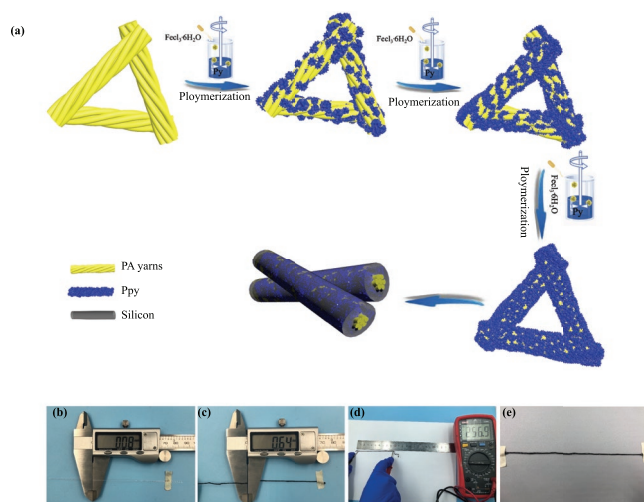


Figure 1. Schematic diagram. a) Schematic showing the preparation of PA-PPy yarn and EMS-TENG. b,c) The diameter of PA and PA-PPy₇ yarn. d,e) Resistance of PA-PPy₇ yarn and the photograph of EMS-TENG.

a part of wearable electronics, have been devoted with tremendous efforts to develop healthcare monitoring, real-time location, and diversified sensing system. In the meantime, human-machine interactions, which consist of energy capture sensing and Internet of Things (IoTs) technology, significantly stimulate the development of wearable textiles. Hence, textiles are undertaking an imperative reformation for multi-function in intelligent wearable applications.^[25–28] As living standard improves, textile, often in close contact with human body, is obtained not only for protective or esthetic but also for functional properties, such as physical/chemical sensing, intelligent interfaces, display, communication, and so on.^[29,30] The previous production of the wearable textiles adopts the approach where textile acts only as the basic substrate for incorporating the rigid or heavy electrical elements. To achieve a seamless integration of specific functions with textiles, inherently soft sensors based on textiles have appeared.^[31,32] Unlike conventional textiles, present functional textiles are gradually sufficient for flexible and easy fabrication products. As a promising candidate, smart textile manufactured by frontiers technology is widely used in cutting-edge technology, such as protective products, military, aeronautics and astronautics, and so on.^[33–36]

Triboelectric nanogenerator (TEG) serves as an emerging energy-harvesting technology that can convert ubiquitous mechanical energy into precious electrical energy, due to the coupling effect of contact electrification and electrostatic induction.^[37–40] TEGs have been verified to capture useless mechanical energies that are omnipresent but otherwise discarded in living surroundings.^[41–45] Thanks to the unique merits of diverse choices of materials, high softness and flexibility, and low cost, TEG is a burgeoning technique for textile-based mechanical energy collection and multifunctional self-powered sensors.^[46–49] Therefore, combining the merits of wearable textile (e.g., conformability, portability, and flexibility) and the TEG technology (e.g., dynamic sensing and self-powered ability), many research have been concentrated on the fabrication of triboelectric and multifunctional textiles. Constructing

versatile device based on textiles can endow them with textiles' merits including flexibility and wearability, facilitating them to withstand intricate changes from uncontrolled forces, and widen their versatile applicability.^[50–52] Moreover, studies of the combination of EMI shielding capability and TENG with energy capture ability are still scarce. Most importantly, the urgency in the implementation and use of green solvents instead of mental materials has driven the application of nontoxic organic liquids towards the development of EMI shielding products.^[53,54]

In this work, we design an electromagnetic shielding-triboelectric nanogenerator (EMS-TENG) with coaxial structure by polymerizing pyrrole (Py) and doping encapsulated material of silicone rubber on the surface of polyamide (PA) yarns that can convert mechanical energy into electrical signals. During the polymerization reaction, Py and ferric chloride are reacted and converted to PPy, forming PA-PPy yarns, which favor them with good EMS ability. The developed EMS-TENG equipped with EMS capacity that can shield undesirable electromagnetic waves effectively. Moreover, the EMS-TENG is a plausible option for harvesting tiny-frequency energies from natural human body movements. In addition, the designed EMS-TENGs are further woven into fabric to construct a dual-functional calculator, which instantaneously identify arithmetic accurately under IoT science. To sum up, with the signals collected from EMS-TENG, and EMS ability as well as additional wearable sensors, this system paves the way to the realization of human-machine interactions and smart wearable technology in near future.

2. Results and Discussion

Electrification materials and electrodes are two indispensable components in TENG system. Yarns treated by physical and chemical method can be used as conductive electrodes. Here, core-shell yarn composed of PA-PPy as the core and silicone rubber as the sheath, as schematically shown in **Figure 1a**, is employed as the building matrix for TENG yarns. **Figure 1b,c** shows the diameters of pure PA yarn and PA-PPy₇ yarn, which are about 0.008 and 0.64 mm, respectively. Through polymerization technique, the PA-PPy₇ yarn is fitness and highly conductive (**Figure 1d**). EMS-TENG is obtained by covering silicon rubber function as an effective insulating layer (**Figure 1e**).

To intuitive comprehend charge transfer process during the contact separation movement, the operating principle of the single-electrode EMS-TENG is discussed (**Figure 2a**). In the EMS-TENG system, the rubber and the PA-PPy yarn function as dielectric and conductive electrode, respectively. In the original mode, when the device is touched with object, charges are transferred from object to the device owing to the stronger performance to accumulate negative charges of rubber. No charge transfer happens at this stage due to the lack of electrical potential difference (**Figure 2a-i**). When the separation occurs, the negative charges from the outer of the EMS-TENG induce positive charges, bringing about free electrons flow from electrode to the ground, thereby producing an instantaneous electrical current (**Figure 2a-ii**). When object is separated with the EMS-TENG continuously, the equilibrium condition is constructed and electrons in the EMS-TENG are balanced,

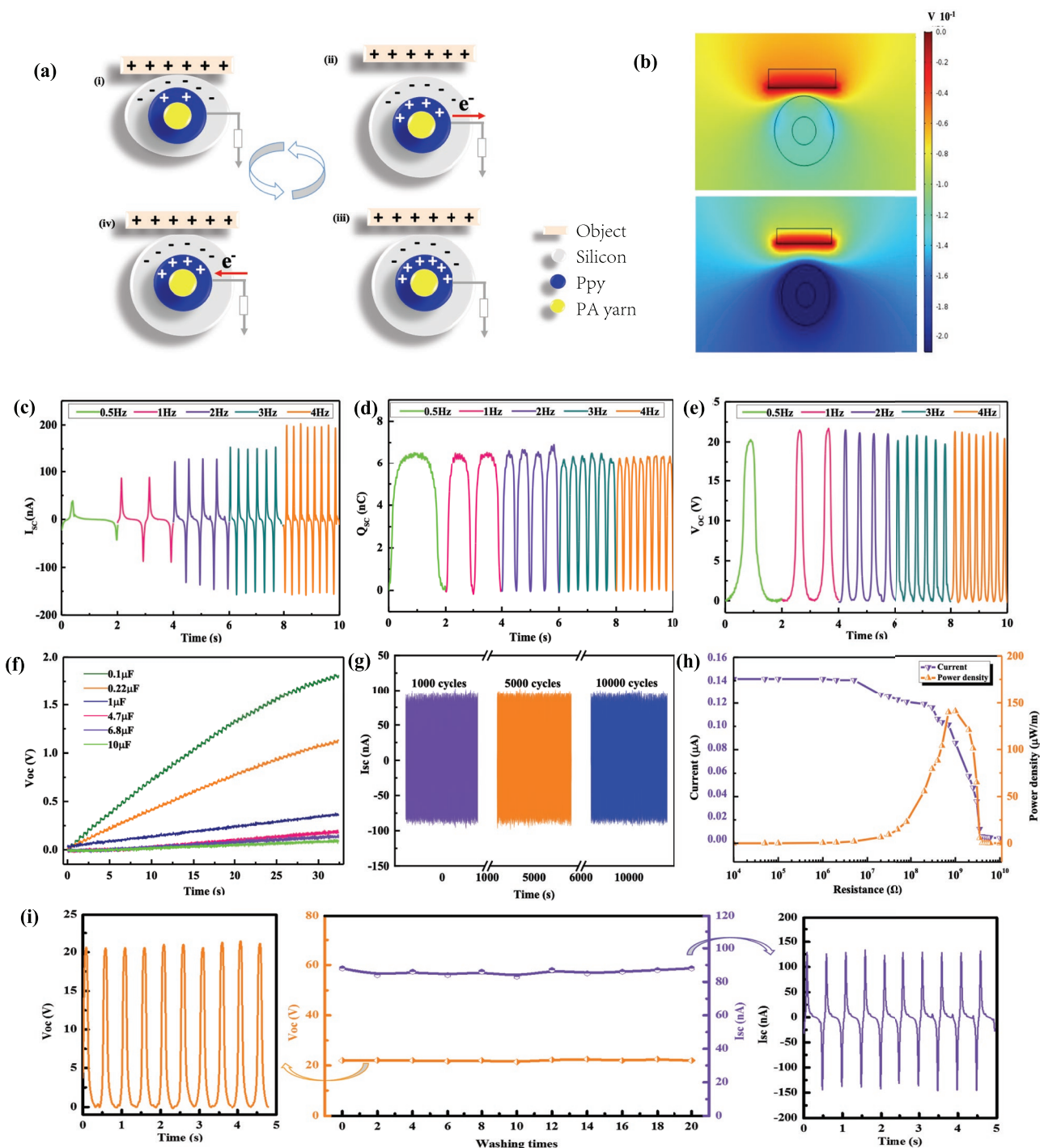


Figure 2. Working mechanism and performance of the EMS-TENG. a) The working principles of EMS-TENG (i–iv). b) The potential distributions for EMS-TENG at different states simulated by COMSOL software. Performance of EMS-TENG: c) short-circuit current, d) open-circuit voltage, and e) short-circuit charge quantity of EMS-TENG at different frequencies. f) The capacitor charging ability of the EMS-TENG under 1 Hz frequency and 10 N force. g) Stability of open-circuit voltage over 10 000 cycles. h) The current and peak power of the EMS-TENG measured with different external load resistances under 1 Hz. i) The output performance of EMS-TENG under different washing time.

leading to no electron movements (Figure 2a-iii). As the EMS-TENG contacting with the device again, electrons transfer from the ground to the inner electrode to achieve electrical potential equilibrium (Figure 2a-iv). When object completed touches

with the EMS-TENG again, no electrical signal can be detected. Therefore, through repeating the contact-separation process, the EMS-TENG can produce an instantaneous alternating potential and current continuously. The electrostatic potential

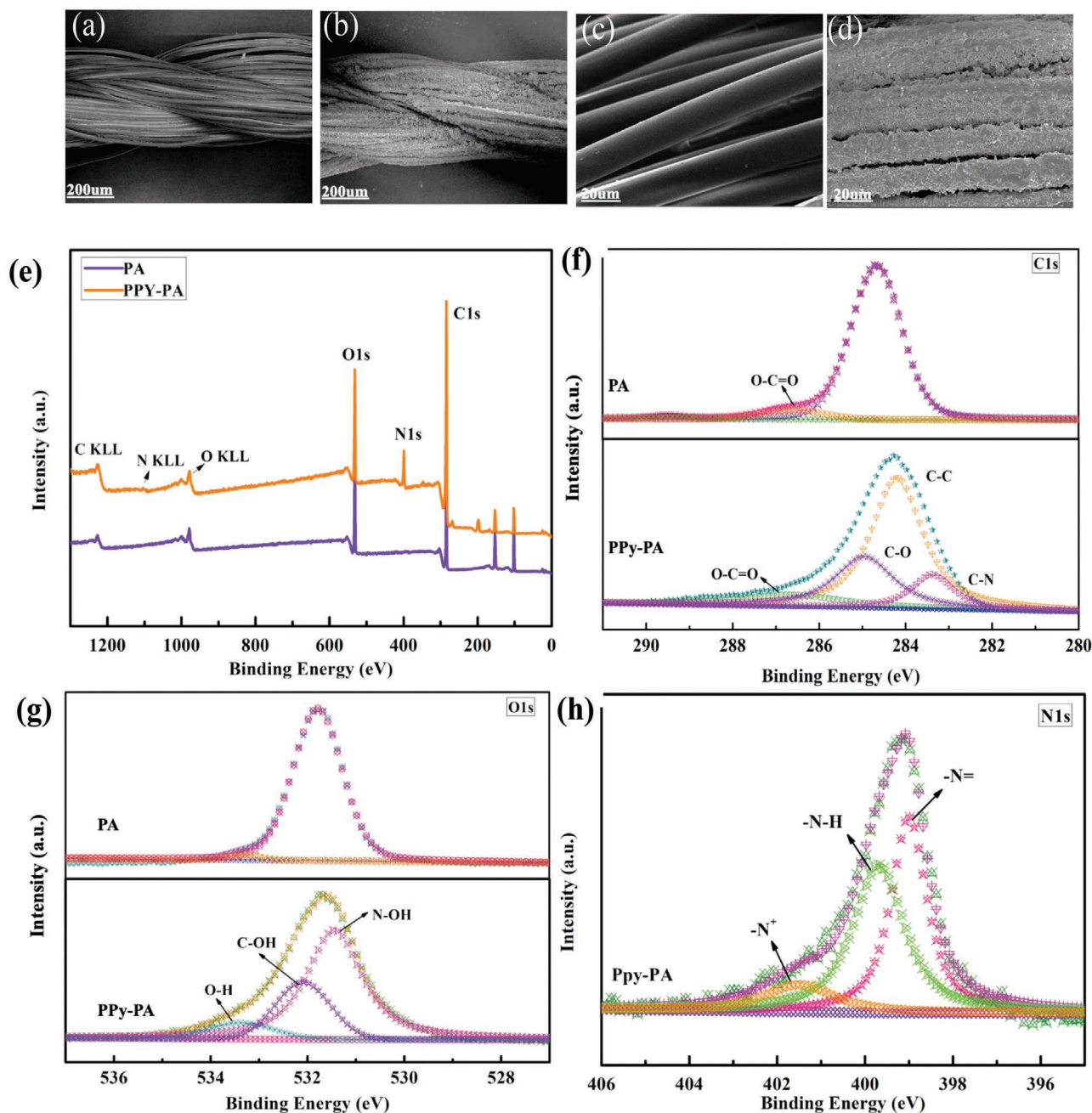


Figure 3. Performance of PA and PA-PPy yarn. a, b) SEM images of PA and c, d) PA-PPy yarns. XPS spectra of PA and PA-PPy yarn. e) Survey spectrum, f) C1s, g) O1s, and h) N1s.

distribution in the contact-separation movement simulated by COMSOL is presented in Figure 2b.

The open-circuit voltage (V_{OC}), the short-circuit current (I_{SC}), and the short-circuit charge quantity (Q_{SC}) of EMS-TENG under working frequency ranging from 0.5 to 4 Hz are shown in Figure 2c–e. It is interesting that a single yarn with a length of 5 cm can generate a high electrical performance (22 V, 48 nA, and 6.8 nC) under low frequency of 0.5 Hz. However, the peak value of I_{SC} increases distinctly from 48 to 208 nA with raising the operation frequency, revealing that the increase of

frequency provides a favorable effect that greatly enhances the output property of I_{SC} . Furthermore, under various working frequencies, the V_{OC} and Q_{SC} still maintain constant ≈ 22 V and ≈ 6.8 nC, no obvious changes can be observed. Figure 2e depicts the charging ability of EMS-TENG under different capacitors. It shows that the charging rate promotes with decreasing the capacitance. In addition, the stability of EMS-TENG is also tested (Figure 2g). It can be found that the I_{sc} has no decay in constant operation of 10 000 cycles, directly demonstrating the robust stability of EMS-TENG. To investigate the output

property of the EMS-TENG, the output current is tested by applying different resistances as the external loads (Figure 2h). The output current decreases with increasing the applied external resistances, it can obtain a maximum peak value of $142.27 \mu\text{W m}^{-1}$ as the external load resistance is about $1 \text{ G}\Omega$.

Washability is a fundamental property for textiles in their practical application.^[55] Thus, the washability of EMS-TENG was examined by immersing it into deionized (DI) water with detergents under constant stirring. After 20 consecutive wash experiments, the electrical output performance of EMS-TENG exhibits no obvious reduction, confirming that EMS-TENG have good washing durability and can be repeatedly used in practical applications (Figure 2i).

The morphological structures of PA and PA-PPy yarns are shown in Figure 3. It is shown that pure PA yarn presents smooth surface with parallel stripes (Figure 3a,b). For PA-PPy yarn, after in situ polymerization synthesis, the existence of PPy clusters is well verified. The scanning electron microscopy (SEM) images of PA-PPy yarn exhibit that PPy particles are closely deposited on the surface of PA, which endow PA-PPy yarn great EMI capacity, demonstrating that PA and PPy are well coupled together (Figure 3c,d).

X-ray photoelectron spectroscopy (XPS) technique is a powerful tool for further delving the interaction of PPy and PA yarn, as presented in Figure 3. The full survey spectra of PA and PA-PPy yarn (Figure 3e) reveal that the existence of elements C, N, O on the surface of both PA and PA-PPy yarn and the respective atomic content for PA-PPy is 75.23%, 8.78%, and 15.98% (Table S1, Supporting Information).

Because of the introduction of PPy, the intensity of C and N on the interface of PA-PPy yarn becomes stronger when compared with that of PA yarn. In addition, the data of the XPS of PA and PA-PPy yarn are displayed in Figure 3f–h. For the C1s spectrum of PA yarn, the spectrum can be divided into two peaks at 284.3 and 286 eV, assigning to C–C and O–C=O bonds, respectively. In the spectrum of PA-PPy yarn, the peaks at 284.3 and 286 eV are still detected. Besides, the two peaks responsible for C–O and C–N are also captured, demonstrating the formation of functional groups due to the addition of PPy. The O1s spectra of both PA and PA-PPy exhibit the typical C–OH (533.2 eV) and N–OH (531.6 eV) groups. Notably, the C–OH contents of PA-PPy dramatically increase, which are larger than that of pure PA yarn. Moreover, two new shoulder peaks at 531.45 eV (N–OH) and 533.4 eV (O–H) are obviously occurred, further verifying the polymerization of PPy on PA yarn. Figure 3h shows the N1s XPS of PA-PPy, where three peaks situated at 399, 399.7, and 401.5 eV can be attributed to –N=, –N–H, and –N⁺ bonds in PPy, respectively.

The X-ray diffraction (XRD) patterns of PA and PA-PPy yarn are displayed in Figure S1 (Supporting Information). The pattern of PA yarn exhibits three peaks centered at 17.9° , 23.3° , and 26.5° , which are attributed to the α phase of PA. The peaks of PA-PPy yarn are almost identical to those of PA without any shift, indicating that the polymerization of PPy will not affect the structure of PA yarn. Most importantly, the peaks of PA-PPy yarn become relatively broader and weaker with the deposition of PPy, meaning the presence of PPy onto PA yarn.

EMI shielding means to isolate or weaken electromagnetic waves outside the shielded area by shielding body to reduce or

eliminate the adverse effects of electromagnetic waves on sensitive equipment, devices or human body within the shielded area (Figure 4a). To quantify the feasibility of EMI shielding for smart textiles, the prepared EMS-TENG was fabricated into a smart fabric with plain woven structure. The overall SE_T is the sum of the reflection loss (SE_R), absorbing loss (SE_A), as calculated in equation^[56,57]

$$SE_T = SE_R + SE_A \quad (1)$$

$$SE_R \text{ (dB)} = -10 \ln(1 - R) \quad (2)$$

$$SE_A \text{ (dB)} = -10 \ln(T / (1 - R)) \quad (3)$$

As depicted in Figure 4a, pure PA fabric is almost transparent to electromagnetic wave within X-band, suggesting that pure PA fabric has negligible electromagnetic shielding capacity. By assembling PPy, the SE_T performance of EMS-TENG fabric is effectively enhanced, which attributes to the construction of the conductive network of PPy. This indicates that PPy plays a key role in promoting EMI ability of EMS-TENG fabric. While the SE_T values of EMS-TENG fabric reveal an increasing trend with increasing the number of self-assembled layers, illustrating that the introduction of PPy has a positive influence on improving EMI performance. Especially, the total shielding effectiveness of EMS-TENG (7BL) fabric is 32.49 dB, proving that above 99.9% of the electromagnetic waves can be shielded, which can meet the demand for commercial applications (20 dB). Based on the formula, SE_T is composed of SE_R and SE_A . As shown in Figure 4c,d, both SE_R and SE_A increase with the increase of self-assembled layers. Noticeably, the SE_A value is significantly higher than SE_R , which manifests that the SE_T ability mainly originates from the contribution of SE_A instead of SE_R , verifying that the shielding mechanism for PPy is absorption. Generally, the real part (ϵ' , μ') and the imaginary part (ϵ'' , μ'') represent the storage ability and dissipation of electromagnetic energy, respectively. Figure 4e,f shows the complex permittivity and complex permeability of EMS-TENG fabric with different self-assembled layers. The ϵ' and ϵ'' of pure PA fabric are about 7 and 0.2, respectively, indicating that PA fabric presents the low dielectric loss capability. The increase of the self-assembled layers results in notably enhancing in ϵ' and ϵ'' , which ascribes to the improved conductivity of EMS-TENG. Thus, the higher dielectric loss of EMS-TENG (7BL) fabric may be due to their relative higher electrical conductivity. Simultaneously, Figure 4g,h shows that the μ' and μ'' decrease with the increase of self-assembled layers except for pure PA fabric. In addition, the dielectric loss and magnetic loss can also be calculated by dielectric loss tangent ($\tan \delta_\epsilon$) and magnetic loss tangent. As expressed in equation^[58]

$$\tan \delta_\epsilon = \frac{\epsilon''}{\epsilon'} \quad (4)$$

$$\tan \delta_\mu = \frac{\mu''}{\mu'} \quad (5)$$

The dielectric loss ($\tan \delta_\epsilon$) increases but the magnetic loss ($\tan \delta_\mu$) decreases (Figure 4h,i) with the enhanced self-assembled

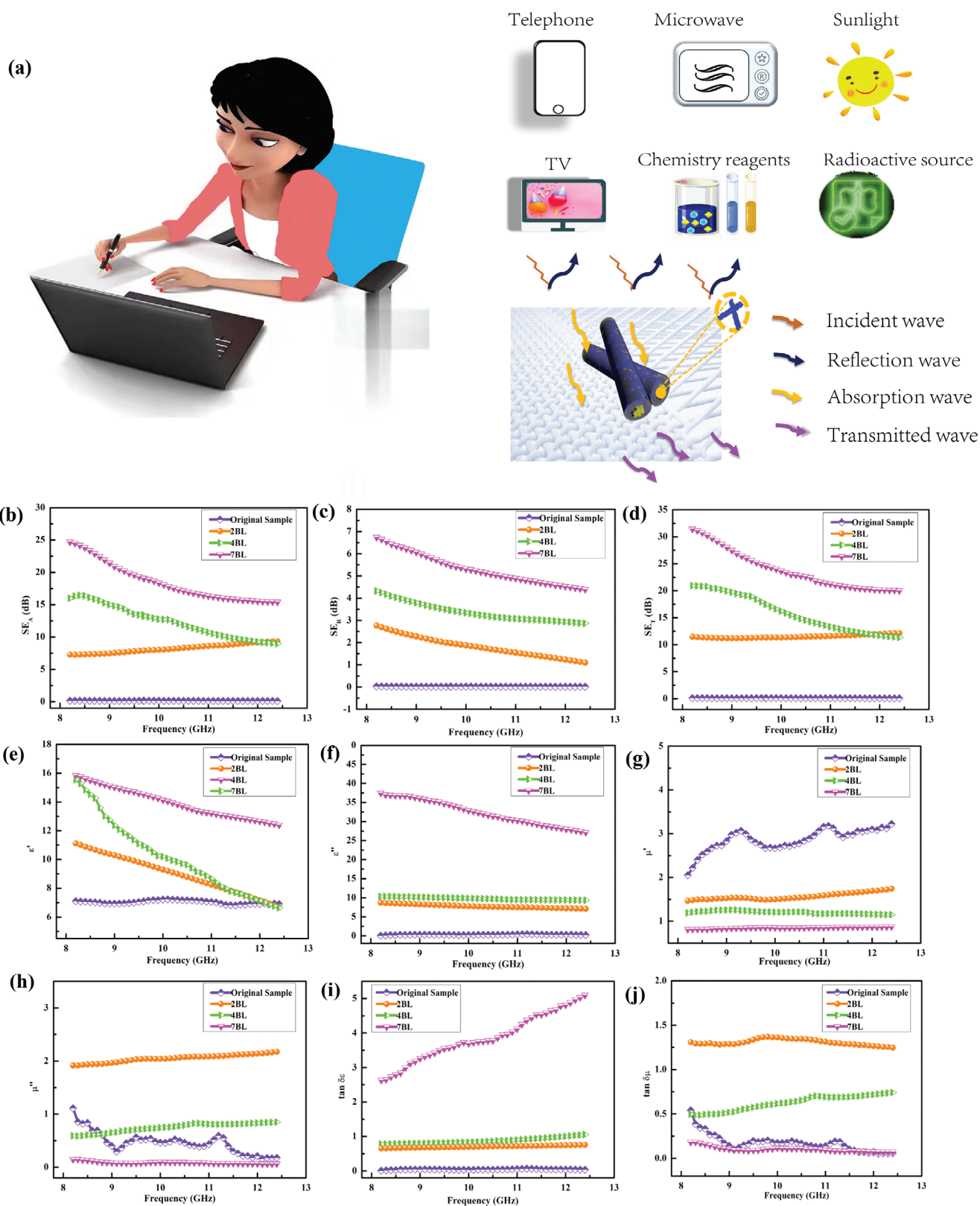


Figure 4. EMS performance of the fabric woven by EMS-TENG. a) Schematic showing the EMI shielding effect for EMS-TENG fabric. b) EMI SE_A , c) EMI SE_E , and d) EMI SE_R of EMS-TENG fabric with different PPy contents. e) Real part of dielectric permittivity (ϵ'). f) Imaginary part of dielectric permittivity (ϵ''). g) Real part of magnetic permeability (μ'). h) Imaginary part of magnetic permeability (μ'') of EMS-TENG fabric with different PPy contents. i) Dielectric loss tangent of EMS-TENG fabric with different PPy contents. j) Magnetic loss tangent of EMS-TENG fabric with different PPy contents.

layers, reflecting that dense conductive network greatly improves the conductivity and thus results in a high dielectric loss capability. When the conductivity of EMS-TENG fabric is relatively low, good impedance matching enables EM waves to enter the material and be absorbed by routes of dielectric loss and magnetic loss. While the significantly improved conductivity of EMS-TENG fabric leads to a serious impedance mismatch. This result clearly demonstrates that the dense conductive network greatly improves the conductivity and thus leads to the high dielectric loss capability (Figure S2, Supporting Information). Therefore, the EMS-TENG (7BL) fabric exhibits high efficiency shielding performance. Despite the different EMI capacity observed for the EMS-TENG fabric, the SE_T , SE_A , and SE_R value for each EMS-TENG fabric increase with enhancing the amount of PPy (Figure S3, Supporting Information).

Alongside with the enormous expansion of the IoT science, integrating IoT with TENG sensor has been exploited to obtain intelligent recognition and detection automation. For verifying the advanced function of recognition and conversion system based on TENG combining with IoT, different types of function are displayed in Figure 5. In general, it is indispensable to identify the output signal directly acquired by TENG and the overall data processing scheme is shown in Figure 5a. A sensor with the intersections similar to the commands on a calculator is designed by EMS-TENG (warp yarns: 5–7, and weft yarns: 1–4) together with common yarns, to simulate an intelligent calculator for simple arithmetic analysis (Figure 5b,d). As illustrated in Figure 5b, each EMS-TENG connects to one channel. By slight touching the point on the two crossed EMS-TENG yarns, the corresponding command can be identified and analyzed via the output voltages of EMS-TENG. Hence, the output signals of “69/3” and “5 × 4” are tested for smart recognition and calculation (Figure S4 and Movies S1 and S2, Supporting Information). And each signal regarding to an Arabic number and symbol is shown in Figure 5e, from which the corresponding results both “multiply” and “divide” can be accurately calculated (Figure 5c,e). Moreover, due to the good EMI shielding performance and self-powered sensing, some tiny vibrations of features can be acquired based on the produced voltage signals on both the output frequencies and their relative magnitudes. In addition to touch sensing, the EMS-TENG is adopted for tracking motions and collecting mechanical energy from our daily activities. Figure 5f,g exhibits the output signals of an individual operating various types of movements, for instance, slow walking, fast walking, slight finger bending, and vertical finger bending with EMS-TENG. The specific signal curves for the normal walking and running process are shown in Figure 5f. In the case of running with the output voltage of 3.8 V, owing to the fast frequency (exceeds to 3 Hz) applied on the knee joint, the warning green light is turn on consequently (Figure S5, Supporting Information). Similarly, concerning the energy tracking, the EMS-TENG is assembled on the finger to capture mechanical energy from the motion of joint. The signal amplitude of V_{oc} rises from 0.5 to 4 V with the change of finger joint angle from 30° to 90°, indicating the output performance of EMS-TENG accelerates with increasing the finger joint angles (Figure 5g). EMS-TENG easily distinguishes the different types of activities according to the overall magnitude and frequency of the output signals, suggesting the great activity

monitoring ability. Overall, in this demonstration, both EMS ability and mechanical energy collection using EMS-TENG can be successfully achieved, implying the great potential of the EMS-TENG in smart wearable and self-powered sensor.

3. Conclusion

In summary, the EMS-TENG is successfully developed for EMS and activity monitoring toward the wearable system. The EMI shielding textile-based TENG that can simultaneously convert energy for human movements is presented. The EMS-TENG achieves high outputs (22 V, 208 nA, and 6.8 nC under the frequency of 4 Hz) and robust stability for 10 000 cycles. Compared with pure PA fabric, the knitted fabric with EMS-TENG triboelectric yarns exhibits a high EMI shielding effectiveness of 32.49 dB. The remarkable capability of energy converting with the EMI shielding property of PA-PPy yarns enable the woven EMS-TENG fabric to monitor signals from human movements, which can benefit to deploy the intelligent EMI protection devices and boost their applicability in electronic communications. This work may build up a promising approach for harvesting energy, sparking the development of wearable textile electronics.

4. Experimental Section

Materials: Ferric chloride ($FeCl_3 \cdot 6H_2O$, 99%), Py, and sodium hydroxide (NaOH) were provided by Aladdin Reagent Company. DI water from ULUPURE pure ultrapure water system was used in experiments.

Preparation of Nylon Fiber Coated with Polypyrrole (PA-PPy): First, 1.677g of Py was added into 25 mL DI water by stirring to obtain a uniform dispersion. Before assembly, PA yarn was washed with detergent in DI water for several times and dried at 60 °C. A typical PA-PPy yarn synthesis process is as follows: PA yarn was immersed into Py suspension for 30 min to adsorption equilibrium with the temperature below 4 °C. 25 mL of $FeCl_3$ solution (1 mol L^{-1}) was mixed into the above suspension and polymerized at 4 °C for 30 min under constant stirring. Then, the synthesized PA-PPy yarn was taken out and washed with DI water thoroughly to remove extra substrate. This cycle presents one bilayer of PA and PPy, and denoted as PA-PPy. Subsequently, the cycle was repeated until the required number of bilayers was reached. Finally, the coated PA yarn was dried under vacuum at 60 °C. For comparison, PA-PPy yarns with different assembly times were also synthesized using the same method, which are termed as PA-PPy x , where x represents the number of polymerization layers.

Preparation of EMS-TENG Yarn: Silicone rubber as the flexible dielectric material was prepared via mixing the two components with the mass of 1:1. The mixture was blended and degassed in vacuum for 10 min to eliminate bubbles. Then, the prepared PA-PPy yarn was uniformly coated by the above mixture. Afterward, the resulting sample was dried at 60 °C for 30 min, and the EMS-TENG was obtained.

Fabrication of EMS-TENG Fabric: EMS-TENG plain stitch fabric with the dimension of 3 cm × 11 cm was fabricated by a simple self-designed mold. The method simulates the mature knitting technology which was presented in modern textile industry and met the requirement of mass production. Briefly, knitted structure were progressively built up by converting newly fed yarn into new loops in the needle hooks, and the needles draw the new loops head first through the ahead loops which they have retained from the previous knitting cycle.

Characterization: The morphology and microstructure images were observed by SEM (su1510 microscope). The crystal structure was characterized by XRD (Bruker AXS) under $Cu K\alpha$ radiation in the range 10°–90°. XPS (Thermo ESCALAB 250Xi) with a base vacuum operated at

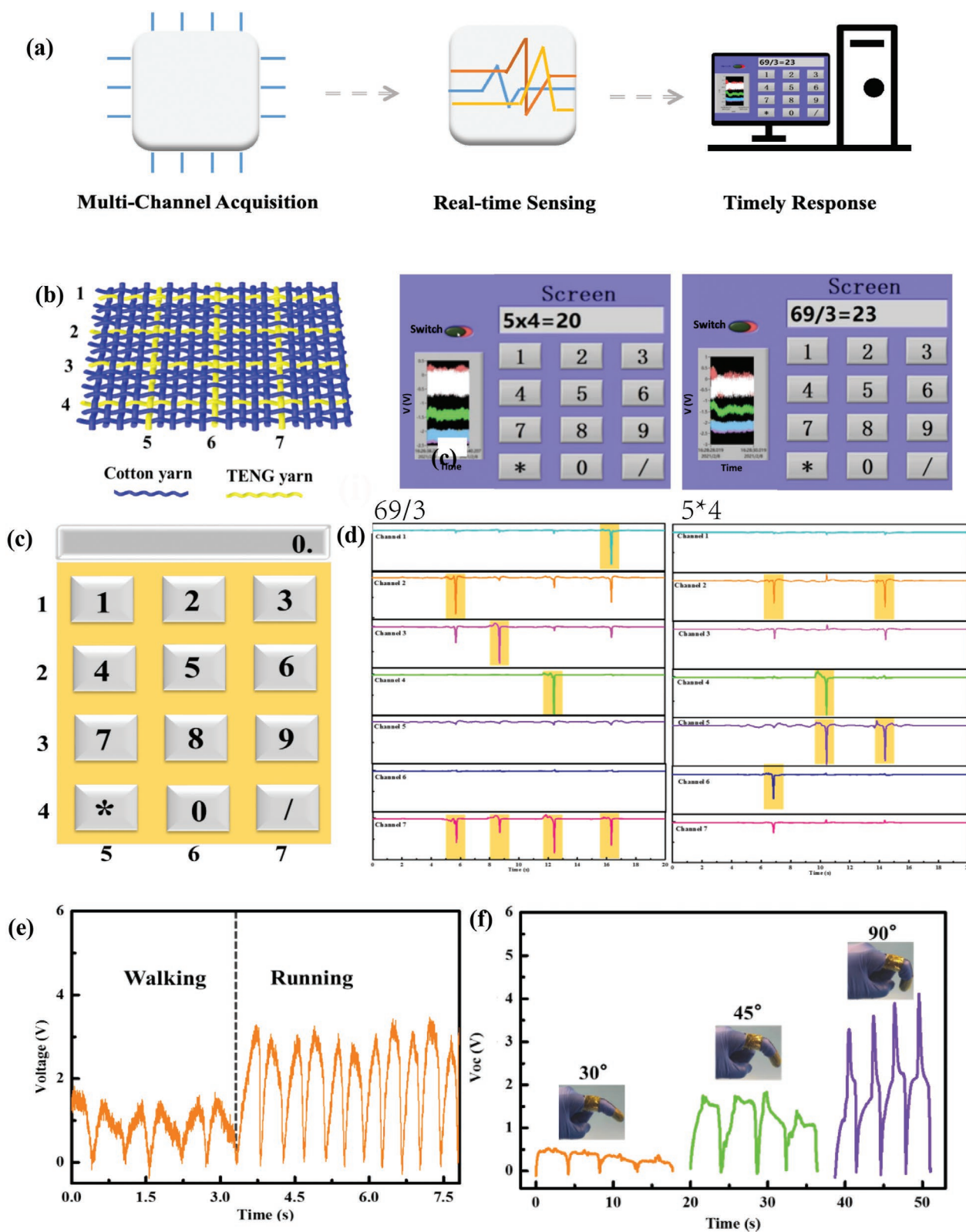


Figure 5. Functional application and sensing features and of EMS-TENG. a) Schematic illustration of the operation of the tactile sensor arrays for real-time arithmetic tracking. b) Photograph of EMS-TENG-based tactile sensor array with the dimension of $12 \times 12 \text{ cm}^2$. c) The real-time arithmetic calculation of EMS-TENG as a smart calculator. d) Diagram of calculator based on tactile sensor array. e) Signal output waveform by entering the division of “69/3” and the multiplication of “ 5×4 ”. f) Voltage signals of EMS-TENG attached on knee under walking and running states. g) The voltage peak value of EMS-TENG under different finger bending angles, including 30° , 45° , and 90° .

300 W was used to detect the chemical environments and interactions. EMI shielding measurement was conducted on an Agilent Technologies E5071C vector network analyzer. The electronic output performance was measured by an electrometer (Keithley 6514).

Data Collection and Training Model: The produced triboelectric signals from the EMS-TENG fabric were achieved by the signal acquisition module in LabView in a real-time manner. In terms of training data for calculating, the signal data from each point were recorded with two channels, and 12 points were separately connected to seven channels in total.

Supporting Information

Supporting Information is available from the Wiley Online Library or from the author.

Acknowledgements

This study was financially supported by National Natural Science Foundation of China (Grant No. 22109012), Natural Science Foundation of the Beijing Municipality (Grant No. 2212052), the Fundamental Research Funds for the Central Universities (Grant No. E1E46805), National Key R&D Program of China (Grant Nos. 2016YFA0202704 and 2019YFA0706900), China Postdoctoral Science Foundation (Grant No. 2019T120390), and Jiangsu Planned Projects for Postdoctoral Research Funds (Grant No. 2018K018A). The authors would also like to thank Shiyanjia laboratory (www.shiyanjia.com) for their professional tests support.

Conflict of Interest

The authors declare no conflict of interest.

Author Contributions

S.S., K.D., and Z.L.W.: Conceived and designed the research. S.S. and K.D. conducted the experiment and characterization. J.Y., L.M., F.S., H.L., R.C., C.N., and Y.Z.: Helped the material synthesis and data processing. H.W., K.D., and Z.L.W.: Supervised, reviewed, and edited the research. All authors discussed and analyzed the data. S.S., K.D., and Z.L.W. co-wrote the paper.

Data Availability

The data that support the findings of this study are available from the corresponding author upon reasonable request.

Keywords

digital numbers, electromagnetic shielding, human-interactive sensing, Internet of Things (IoTs), triboelectric nanogenerators

Received: October 16, 2021

Revised: November 19, 2021

Published online:

[1] L. Xiang, A. Yz, B. Jy, A. Jq, *Composites, Part B* **2020**, 199, 108308.

[2] H. N. Yoon, D. Jang, H. K. Lee, I. W. Nam, *Constr. Build. Mater.* **2020**, 269, 121238.

- [3] G. Yin, Y. Wang, W. Wang, D. Yu, *Colloids Surf., A* **2020**, 601, 125047.
- [4] J. Lu, Y. Zhang, Y. Tao, B. Wang, Y. Hu, J. *Colloid Interface Sci.* **2020**, 588, 164.
- [5] Y. Gao, Z. Wang, J. *Magn. Magn. Mater.* **2021**, 528, 167808.
- [6] S. Kasisomayajula, N. Jadhav, V. J. Gelling, *Prog. Org. Coat.* **2021**, 154, 106190.
- [7] A. Hz, B. Kfa, A. By, L. A. Yan, *Compos. Sci. Technol.* **2021**, 207, 108675.
- [8] S. Ghayempour, M. Montazer, *Cellulose* **2016**, 23, 2561.
- [9] S. D. Ramoa, G. M. Barra, R. V. Oliveira, M. G. de Oliveira, M. Cossa, B. G. Soares, *Polym. Int.* **2013**, 62, 1477.
- [10] B. Cho, H. Lim, H. N. Lee, Y. M. Park, H. J. Kim, *Surf. Coat. Technol.* **2021**, 407, 126797.
- [11] B. Yza, A. Zs, J. A. Liang, C. Sca, B. Jma, D. Fza, *Appl. Surf. Sci.* **2020**, 533, 147431.
- [12] R. Peymanfar, M. Yektaei, S. Javanshir, E. Selseleh-Zakerin, *Polymer* **2020**, 209, 122981.
- [13] Y. Y. Wang, W. J. Sun, D. X. Yan, K. Dai, Z. M. Li, *Carbon* **2021**, 176, 118.
- [14] W.-L. Song, M.-S. Cao, M.-M. Lu, S. Bi, C.-Y. Wang, J. Liu, J. Yuan, L.-Z. Fan, *Carbon* **2014**, 66, 67.
- [15] L. Kong, X. Yin, H. Xu, X. Yuan, T. Wang, Z. Xu, J. Huang, R. Yang, H. Fan, *Carbon* **2019**, 145, 61.
- [16] J. Joseph, P. R. Munda, D. A. John, A. M. Sidpara, J. Paul, *Mater. Res. Express* **2019**, 6, 085617.
- [17] Y. Han, Y. Liu, L. Han, J. Lin, P. Jin, *Carbon* **2017**, 115, 34.
- [18] Y. Zhang, K. Ruan, X. Shi, H. Qiu, J. Gu, *Carbon* **2020**, 175, 271.
- [19] A. P. Narayanan, K. Unni, K. P. Surendran, *Chem. Eng. J.* **2020**, 408, 127239.
- [20] K. A. Milakin, U. Acharya, M. Trchová, B. A. Zasonska, J. Stejskal, *React. Funct. Polym.* **2020**, 157, 104751.
- [21] Y. Zhang, T. Pan, Z. Yang, *Chem. Eng. J.* **2020**, 389, 124433.
- [22] Y. Ra, J. H. Choi, M. La, S. J. Park, D. Choi, *Funct. Compos. Struct.* **2019**, 1, 045001.
- [23] T. Jin, Z. Sun, L. Li, Q. Zhang, C. Lee, *Nat. Commun.* **2020**, 11, 5381.
- [24] L. Ronghui, A. B. Patil, M. Chen, Z. Zhaohui, X. Yifan, *Text. Res. J.* **2019**, 89, 5144.
- [25] Z. H. Zhou, L. Weng, T. Tat, A. Libanori, Z. M. Lin, L. J. Ge, J. Yang, J. Chen, *ACS Nano* **2020**, 14, 14126.
- [26] K. Dong, Y. Hu, J. Yang, S. W. Kim, Z. L. Wang, *MRS Bull.* **2021**, 46, 512.
- [27] D. Kong, J. Liu, Z. Zhang, S. Wang, Z. Lu, *Cellulose* **2021**, 28, 8115.
- [28] S. Andra, S. K. Balu, J. Jeevanandam, M. Muthalagu, M. K. Danquah, *Cellulose* **2021**, 28, 5895.
- [29] S.-T. Tse, C.-W. Kan, *Cellulose* **2020**, 27, 10385.
- [30] R. Wu, L. Ma, S. Liu, A. B. Patil, X. Y. Liu, *Mater. Today Phys.* **2020**, 15, 100243.
- [31] K. Dong, Y. Hu, J. Yang, S.-W. Kim, W. Hu, Z. L. Wang, *MRS Bull.* **2021**, 46, 512.
- [32] S. T. Liu, H. Wang, T. Y. Y. He, S. R. Dong, C. K. Lee, *Nano Energy* **2020**, 69, 104462.
- [33] B. W. Dong, Q. F. Shi, T. Y. Y. He, Z. X. Zhang, Y. M. Ma, G. Y. Zhou, C. Lee, in *2020 33rd IEEE Int. Conf. on Micro Electro Mechanical Systems*, IEEE, Piscataway, NJ **2020**, pp. 1234–1237.
- [34] J. An, P. Chen, Z. Wang, A. Berbille, H. Pang, Y. Jiang, T. Jiang, Z. L. Wang, *Adv. Mater.* **2021**, 33, 2101891.
- [35] Y. Ji, K. W. Zhang, Y. Yang, *Adv. Sci.* **2018**, 5, 1700622.
- [36] L. Ma, R. Wu, A. Patil, J. Yi, Z. L. Wang, *Adv. Funct. Mater.* **2021**, 31, 2102963.
- [37] Y. Jia, D. Kai, S. Shen, J. Yang, Y. Cui, Z. L. Wang, *Nano-Micro Lett.* **2021**, 13, 103.
- [38] W. X. Liu, Y. M. Ma, Y. H. Chang, B. W. Dong, J. X. Wei, C. K. Lee, in *34th IEEE Int. Conf. Micro Electro Mechanical Systems IEEE*, Piscataway, NJ **2021**, pp. 302–305.
- [39] M. Bouza, Y. Li, A. C. Wang, Z. L. Wang, F. Fernández, *Anal. Chem.* **2021**, 93, 5468.

- [40] T. Jin, Z. D. Sun, L. Li, Q. Zhang, M. L. Zhu, Z. X. Zhang, G. J. Yuan, T. Chen, Y. Z. Tian, X. Y. Hou, C. Lee, *Nat. Commun.* **2020**, *11*, 5381.
- [41] B. W. Dong, Y. Q. Yang, Q. F. Shi, S. Y. Xu, Z. D. Sun, S. Y. Zhu, Z. X. Zhang, D. L. Kwong, G. Y. Zhou, K. W. Ang, C. K. Lee, *ACS Nano* **2020**, *14*, 8915.
- [42] J. X. Zhu, H. Wang, Z. X. Zhang, Z. H. Ren, Q. F. Shi, W. X. Liu, C. K. Lee, *Nano Energy* **2020**, *73*, 104760.
- [43] J. Luo, W. Gao, Z. L. Wang, *Adv. Mater.* **2020**, *33*, 2004178.
- [44] Y. Jia, Y. Pan, C. Wang, C. Liu, C. Shen, C. Pan, Z. Guo, X. Liu, *Nano-Micro Lett.* **2021**, *13*, 201.
- [45] Q. Qiu, M. M. Zhu, Z. L. Li, K. L. Qiu, X. Y. Liu, J. Y. Yu, B. Ding, *Nano Energy* **2019**, *58*, 750.
- [46] M. N. Lou, I. Abdalla, M. M. Zhu, X. D. Wei, J. Y. Yu, Z. L. Li, B. Ding, *ACS Appl. Mater. Interfaces* **2020**, *12*, 19965.
- [47] Y. C. Shao, M. L. Shen, Y. K. Zhou, X. Cui, L. J. Li, Y. Zhang, *Beilstein J. Nanotechnol.* **2021**, *12*, 680.
- [48] E. Li, Y. Pan, C. Wang, C. Liu, C. Shen, C. Pan, X. Liu, *Chem. Eng. J.* **2021**, *420*, 129864.
- [49] Y. M. Liu, L. Y. Wang, L. Zhao, X. G. Yu, Y. L. Zi, *Infomat* **2020**, *2*, 318.
- [50] J. M. Han, M. Wang, Z. M. Tong, Y. F. Ma, *J. Inorg. Mater.* **2019**, *34*, 839.
- [51] S. G. Li, Y. Q. Tan, J. X. Xue, T. Liu, X. S. Zhou, H. B. Zhang, *AIP Adv.* **2018**, *8*, 015027.
- [52] D. J. Jiang, H. Ouyang, B. J. Shi, Y. Zou, P. C. Tan, X. C. Qu, S. Y. Chao, Y. Xi, C. C. Zhao, Y. B. Fan, Z. Li, *Infomat* **2020**, *2*, 1191.
- [53] J. Hong, P. Xu, *Materials* **2021**, *14*, 1907.
- [54] R. Cao, X. Pu, X. Du, W. Yang, J. Wang, H. Guo, S. Zhao, Z. Yuan, C. Zhang, C. Li, *ACS Nano* **2018**, *12*, 5190.
- [55] Y. Fei, M. Liang, T. Zhou, Y. Chen, H. W. Zou, *Carbon* **2020**, *167*, 575.
- [56] H. Jia, Q. Q. Kong, X. Yang, L. J. Xie, G. H. Sun, L. L. Liang, J. P. Chen, D. Liu, Q. G. Guo, C. M. Chen, *Carbon* **2021**, *171*, 329.
- [57] M. N. Qu, X. Yang, L. Peng, L. L. Liu, C. Yang, Z. Zhao, X. R. Liu, T. J. Zhang, J. M. He, *Carbon* **2021**, *174*, 110.
- [58] Q. X. He, R. Chen, S. Li, Z. Y. Wang, F. Y. Wen, B. H. Wang, J. X. Mu, *Composites, Part A* **2021**, *143*, 106280.